J Nanostruct 16(4): 5209-5227, Autumn 2026

RESEARCH PAPER

Harnessing the Sustainable Approach for Copper Nanoparticle Biosynthesis: Investigation of Antiviral and Antioxidant Efficacy and an In Silico Study

Iman A. J. AL-Timimi [1], Mohammed J. Al Yasiri [1]*, Diyar M. A. Murad [1], Amar Yasser Jassim [2], Nawras T. Jassim [3,4], Uche K. Onwukwe [5]

[1] *Department of Chemistry, College of Science, University of Basrah, Basrah, Iraq*

[2] *Department of Marine Vertebrate, Marine Science Center, University of Basrah, Iraq*

[3] *Department of Chemical Engineering, College of Engineering, University of Basrah, Iraq*

[4] *Department of Organic Chemistry and Technologies, Kuban State University, Russia*

[5] *Chemical Engineering, Brunel University London, Uxbridge, Middlesex, UB8 3PH, UK*

ARTICLE INFO

Article History:
Received 27 May 2026
Accepted 28 August 2026
Published 01 October 2026

Keywords:
Antioxidant
Cu-NPs
Docking study
Influenza A virus RNA polymerase 2
SARS-CoV-2
Sustainable Approach

ABSTRACT

The emergence of SARS-CoV-2 and other virus threats has renewed interest in nanoparticles as potential antivirals. Green synthesis of nanoparticles using biological methods offers an eco-friendly, cost-effective alternative to conventional approaches. In this study, copper nanoparticles (Cu-NPs) were biosynthesized using *Artemisia sieberi* (*A.s*) florets extract, which acts as a reducing, capping, and stabilizing agent. The synthesized Cu-NPs/*A.s* were characterized using transmission electron microscopy (TEM), UV–Visible spectroscopy, energy-dispersive X-ray spectroscopy (EDX), and dynamic light scattering (DLS). The antiviral and antioxidant activities of Cu-NPs/*A.s* were evaluated, and molecular docking was performed to explore possible interactions between Cu-NPs/*A.s* with SARS-CoV-2 main protease and influenza A virus RNA polymerase as a hypothesis-generating approach. Structural and morphological characterisations confirmed successful nanoparticle formation, and Cu nanoparticles exhibited smaller particle dimensions (particle size of 63.7 ± 19.5). The Cu-NPs/*A.s* demonstrated notable antioxidant activity (55% scavenging in phosphomolybdate assay) compared to ascorbic acid and a strong inhibitory effect against influenza A virus (IAV) (70.67%). Docking studies indicated favorable binding energy interactions between chlorogenic acid – copper nanoparticles (CGA-Cu NPs /*A.s*) and SARS-CoV-2 are -8.22 kcal/mol; similarly, the influenza A virus (IAV) gives the binding energy -9.22 kcal/mol, which may inform future experimental investigations. The DFT parameters indicate that the Cu-complex possesses favourable electronic properties, a substantial charge transfer capability, and elevated reactivity. To assess organ-specific toxicity, bioavailability and metabolic interactions, a full computational toxicological evaluation using ProTox-3.0 is performed based on a chemical model for a combination hearing aid.

How to cite this article
AL-Timimi I, Al Yasiri M, Murad D, et al . Harnessing the Sustainable Approach for Copper Nanoparticle Biosynthesis: Investigation of Antiviral and Antioxidant Efficacy and an In Silico Study. J Nanostruct, 2026; 16(4):5209-5227. DOI: 10.22052/JNS.2026.04.059

* *Corresponding Author Email: mohammed.jasim@uobasrah.edu.iq*

INTRODUCTION

Nanoparticles (NPs) have gained increasing significance in medical applications, demonstrating antiviral activity against a range of viral diseases [1]. This increase in significance is thought to be due to their unique physicochemical properties, such as electrical conductivity, catalytic active sites, shape, crystalline structure, and their improved surface area/volume ratio, compared to their bulk counterparts [2]. Nanoparticles have become tremendously influential in applications that extend from medical purification, use as therapeutic agents, medical diagnosis, and more [3]. This has encouraged the rapid expansion in this field of study, which emphasizes the importance of synthesis techniques, surface modification, and usage of materials at the nanoscale [4], and their ultimate effect on the applicability of these nanoscale structures. Inorganic nanomaterials have been of wide interest in the biomedical field [5], due to their importance in improving medical treatments [6] aimed at treating various medical conditions [7]. Various inorganic metals such as Au [8], Ag [9], Se [10], Cu, Zn [11] , and metals oxide as TiO_2 [9]and Fe_3O_4 NPs have been used to synthesis nanoparticles, critical in the medical field [12].

Copper nanoparticles (Cu-NPs) are among the nanomaterials that have garnered wide interest due to their importance in modern technologies and their remarkable antimicrobial properties [13]. Different methodologies, including physical, chemical, and biological techniques, have been devised to create nanomaterials with precise sizes, shapes, and stability [14]. The chemical and physical approaches typically produce hazardous byproducts along with their prohibitive costs [15]. Thus, it is crucial to appropriately dispose of these dangerous byproducts, often toxic and corrosive, to reduce the environmental consequences of their manufacture. As the demand for more eco-friendly manufactured nanoparticles have increased [16], the pursuit of alternative means of manufacturing these nanoparticles has also grown to include green processing techniques. These green processing routes commonly utilize microorganisms such as algae [17], bacteria, fungi, and the various parts of plants to synthesis and stabilise these nanoparticles [18]. In these green routes, plants are preferred for nanoparticle synthesis over other biological sources, due to their wide availability, simplicity of handling, and their variety of metabolites (as polysaccharides,

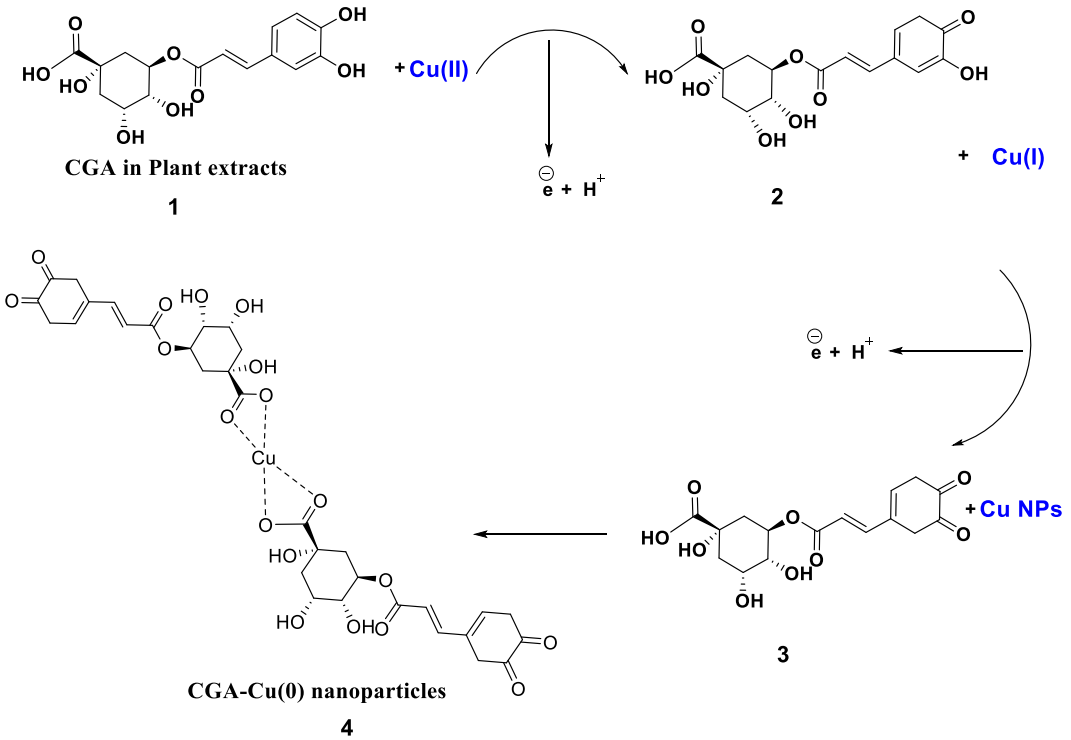

Fig. 1. A suggested mechanism for converting copper salt into copper nanoparticles (CGA=1, and CGA–Cu complex = 4).

proteins, alkaloids, flavonoids, fatty acids, and others) [19] that can mediate the synthesis process. These bioactive chemicals behave like stabilizing, reducing, and capping agents in the biosynthesis of these nanoparticles [20]. Various parts of a plant, such as leaves, roots, seeds, peel, flowers, and stems, are typically used for the preparation of Cu-NPs [21].

Artemisia sieberi (A.s) is an important medicinal plant that is currently the subject of interest because of its biological and chemical diversity [22]. The screening of *Artemisia* extracts has led to the discovery of many derivatives such as artemisinin, chlorogenic acid (1), kaempferol, and rutin; and whole aerial parts extracts of *Artemisia* species have proven to be effective against many types of viruses, including the COVID 19 [23].

Chlorogenic acid (CGA) (1), an ester of caffeic and quinic acids, is a polyphenol prevalent in Artemisia sieberi extract, with 5-O-caffeoylquinic acid (5-CQA) as its primary isomer. CGA (1) is regarded as a crucial component, demonstrating a diverse array of biological actions, including antioxidant, anti-inflammatory, anticancer, antibacterial, hepatoprotective, cardioprotective, and neuroprotective properties, as well as the control of lipid and glucose metabolism. CGA (1) exhibits significant chelating capabilities, allowing it to form stable complexes with transition metals like Zn(II), Fe(III), Pb(II), and Cu(II) [24]. These CGA-metal complexes demonstrate significant potential in diverse domains, including bioactive drugs, catalytic materials, and environmental remediation tools. The capacity of CGA (1) to chelate metal ions renders it an ideal candidate for the creation of bio-inspired metal complexes. A proposed mechanism for the formation of a primary chlorogenic acid-copper complex is depicted in Fig. 1. Chlorogenic acid (CGA) (1) molecules first reduce Cu^{2+} cations to their metallic state, enabling metallic copper nanoparticles to coordinate with accessible functional groups (i.e., carboxylates) in the CGA (1) network, therefore forming the CGA–Cu complex (4) [25].

The biomedical use of NPs as antiviral agents are thought to be due to certain key mechanisms: i) the direct interaction with viruses, which prohibits them from infecting cells of the virus; ii) the interaction with receptor or other cell surface moieties to prevent virus entry into host cells; iii) prevention of viral cell replication; (iv) inhibition of viral spread [26,27]. Current antiviral drugs are only effective against limited types of viruses, e.g., the influenza and COVID-19 virus. Recently, many studies have focused on using metal nanoparticles, especially Au NPs [27] and Ag NPs, and others in combination with natural biomolecules as antiviral agents for treatments. Several natural inhibitory chemicals as well as nanoparticles have been studied to understand their irreversible ability to bind to the active site of viral enzymes. The investigation examines the suppressive impact on enzymatic activity and the consequent obstruction of viral proliferation [28].

A recently emerged and fatal variation of COVID-19, identified as SARS-CoV-2, has arisen due to its fast transmission from human to human, with confirmed cases in every country. This study focuses on the eco-friendly synthesis of copper nanoparticles (Cu-NPs/*A.s*) and chlorogenic acid – copper nanoparticles (CGA-Cu NPs /*A.s*) and evaluates their virucidal activity against influenza A virus as well as their antioxidant potential. Additionally, the interactions of Cu-NPs/*A.s* and CGA-Cu NPs /*A.s* were investigated against SARS-CoV-2 (PDB ID: 8DZ2) and influenza A virus RNA polymerase (PDB ID: 6FS6) through molecular docking to identify a potential antiviral candidate. The objective is to identify an appropriate antiviral candidate that can specifically target SARS-CoV.

MATERIALS AND METHODS

Materials

Brown fresh flowers *A.s* were purchased from the local markets at Basrah, Iraq. The reagents used included copper chloride [$CuCl_2$, HIMDI, 99%].

The antioxidant activity reagents were ammonium molybdate ($(NH_4)\ 6Mo_7O_{24}.4H_2O$; G.P.R, 98%), sodium phosphate, sulfuric acid and standard ascorbic acid (Sigma; 99%). The antiviral activity was tested in MDCK-SIAT1 cells infected with Influenza A virus (IAV) and the Neuraminidase Assay Kit MAK121 was used.

Biosynthesis Cu-NPs

Preparation of the aqueous extract of A.s Florets

The florets of *A.s* were washed using distilled water (DW), air dried. 10 g of dried for 7 days, and crushed in a mortar. *A.s* were powdered and mixed with 100 mL of deionized water under magnetic stirring for 20 mins at ambient temperature. The resulting suspension was cooled to room temperature, and the extract was filtered

using muslin and filter paper. The filtrate of *Ar.s* was refrigerated to maintain stability and prevent denaturation.

Biogenic Synthesis of copper nanoparticles (Cu-NPs/A.s)

The synthesis of Cu-NPs was carried out with aqueous $CuCl_2 \cdot 2H_2O$ (50 mL, 1.0 mM) solution and added dropwise to the aqueous plant extract (5 mL) while stirring at 700 rpm for 2h at RT under an inert atmosphere (Ar). The pH of the suspension was adjusted to around 9-10 by adding NaOH (0.1 and 0.01M). After the pH value was monitored, the reaction mixture was kept at 60°C for 2 h at room temperature with continuous stirring. Completion of the reaction was assessed visually based on the turbidity of the reaction mixture. A color change was noticed, indicating the reduction of metal ions Cu^{2+} to Cu^0 (Cu-NPs/*A.s*). The synthesized Cu-NPs were filtered with a 2.2 µm syringe filter. This reduction was confirmed by a UV-vis spectrophotometer. The Cu-NPs were stored in a refrigerator for further characterization.

Computational Method

Ligands preparation

ChemDraw was used to generate the two-dimensional structure of the chlorogenic acid (CGA-Cu-NPs) complex. The structure was converted into three-dimensional coordinates (PDB format) for docking using Avogadro software and then optimized to achieve minimum energy [29], employing standard parameters. The unit cells of copper nanoparticles were created utilizing the Materials Studio 2017 software library. Molecular mechanics optimizations, including the MM + force field with Hyperchem software, were employed to refine the molecular architecture and subsequently saved in Mol2 format, which is applicable for molecular docking.

Target and Receptor Preparation

The co-crystallised structures of the main protease of SARS-CoV-2 (PDB ID: 8DZ2) in complex with Nirmatrelvir and influenza A virus RNA polymerase (PDB ID: 6FS6) in complex with Baloxavir were retrieved from the RCSB PDB database. The structures were refined using Discovery Studio by removing co-crystallized ligands, water molecules, and cofactors to conduct the procedure. Three-dimensional protonation and energy minimization were performed using the computational option until a gradient of 0.05 was achieved. Polar hydrogen fixation was completed before using it for molecular docking studies.

Docking Procedure (MOE 2019)

Molecular docking studies were conducted on Dell Intel (R) Core (TM) i5-6600U CPU @ 3.30 GHz processor with 238 MB memory and a Windows 10 Pro 64-bit operating system. Docking experiments and analyses were conducted using Molecular Operating Environment (MOE 2019; Chemical Computing Group, Canada) as the computational software. We chose the library's .mdb file and employed the MOE docking module to dock the structural model of the synthesized compounds to the proteins. The docking scores in the MOE program were generated using the London dG scoring function, and the five highest-ranked docked poses were selected for study.

Density Functional Theory (DFT)

Conducting Density Functional Theory (DFT) computations using Gaussian5 is an efficient method for examining molecular characteristics, including stable structures and spectra. Derived from the search outcome [30]. The results from the geometry optimization of the compound were subjected to Frontier Molecular Orbital (FMO) analysis, which includes both the energy of the HOMO and LUMO orbitals. The HOMO-LUMO energies computed with the help of Gaussian 09 have first been expressed in atomic units (Hartree) and then have been converted to eV (1 Hartree = 27.112eV) [31].

Formula used:

chemical potential and chemical hardness to minimize the computational time,

$$\mu = -((IP+EA))/2 \quad (1)$$

$$\eta = ((IP-EA))/2 \quad (2)$$

where, Ionization potential (IP) = - EHOMO and Electron affinity (EA) = - ELUMO. ELUMO and EHOMO are the energies of the lowest unoccupied molecular orbital and the highest occupied molecular orbital, respectively.

The corresponding global softness is expressed as:

$$S=1/2\eta \quad (3)$$

the global electrophilicity index (ω) as follows:

$$\omega = \mu^2/2 \quad (4)$$

Toxicity predicted

ProTox-3.0 is a comprehensive system based on machine learning that classifies compounds as toxic/non-toxic across 61 endpoints, whereas GUSAR is a QSAR system specialized in the quantitative prediction of LD_{50} values with precise determination of result reliability through the concept of the applicability domain. They complement each other: ProTox-3.0 provides a broad picture of different types of toxicity, while GUSAR provides precise numerical values that can be used in quantitative risk assessment.

Basic Principle

ProTox-3.0 is based on integrating molecular similarity with machine learning models to predict 61 different toxicity endpoints. The program analyzes the 2D chemical structure of the input compound and then compares it with large databases of compounds with known toxicity.

On the other hand, the program outputs after the compounds are entered, the ProTox-3.0 program produces the following: classification for each endpoint: active (toxic) or inactive (non-toxic) [32].

Characterization of Cu-NPs/A.s

UV-Vis analysis

Cu-NPs/*A.s* were characterized using a UV-Vis double-beam spectrophotometer (with quartz cuvettes) to confirm the bio-reduction of Cu ions to Cu-NPs. The absorption spectra of biosynthesized Cu-NPs/*A.s* were observed within the range of 200-800 nm.

Fourier Transform Infra-Red Spectroscopy (FTIR)

FTIR analysis was employed to identify the role of biomolecules and their functional groups which are present in the flower extract for the biosynthesis of Cu-NPs/*A.s*. Analysis was carried out within the range of 4000 to 400 cm^{-1}.

Particle size distribution (PSD) and energy-dispersive X-ray spectroscopy (EDX)

The particle size distribution (z-average) of biosynthesized Cu-NPs/*A.s* was measured by dynamic light scattering (DLS) using a Zeta sizer (Nano-ZS, Malvern Instruments Inc). The mean particle sizing (and three independent replicates) was carried out at 25 °C with a detection angle of 90°. Elemental analysis was done using an FE-SEM (TESCAN Mira3) with an EDX detector.

Transmission electron microscopy (TEM)

Surface morphology and particle diameter were examined by TEM (Zeiss EM10C-100 kV). Cu-NPs/*A.s* suspensions were carefully dropped and cast onto a carbon-coated 50 mesh Cu grid and then rinsed with deionized water once dried, to eliminate any particles that had not adhered. Afterwards, the grids were allowed to dry for 48 hours at room temperature. The mean (± the standard deviation) of the particle size distribution data was reported.

Phosphomolybdate antioxidant scavenging activity *assay (PMA)*

The total antioxidant scavenging activity was estimated using a phosphomolybdenum reagent. Phosphomolybdenum reagent was prepared by mixing 4.0 mM ammonium molybdate with 28 mM of sodium phosphate and 0.6 M sulfuric acid. Then, 1 mL of Cu-NPs/*A.s* suspension of different concentrations (6-32 µg/mL) was mixed with 1 mL of phosphomolybdenum and then incubated for 90 minutes in a water bath (95 °C) and then cooled at room temperature. The same experiment without the NP was used as a control. The absorbance was measured at 695 nm. The percentage inhibition of the compound was calculated, and a standard curve of ascorbic acid with the percentage of inhibition was also calculated [33].

Antiviral activity

The neuraminidase assay kit (MAK121) was used to test the antiviral activity of Cu-NPs/*A.s* in Madin-Darby canine kidney (MDCK-SIAT1) cells infected with Influenza A virus (IAV). The antiviral activity experiments were carried out at the Phi-Nano Science Center (PNSC), Baghdad, Iraq.

96 well plates containing 1×10^4 cells underwent pretreatment with varying concentrations (6-32 µg/mL) of Cu-NPs/*A.s* for one hour. Next, the Cu-NPs/*A.s* were rinsed away using a two-step media renewal process. The cells were incubated with the virus at a multiplicity of infection (MOI) of 0.1 for one hour. After 48 hours of infection, the virus was eliminated using neutralizing antibodies, and the amount of new virus was determined by measuring neuraminidase activity. GraphPad Prism

6 software was used for the statistical analysis of the data, which are presented as a mean (± SD) of three replicates per experiment [34].

RESULTS AND DISCUSSION

Green synthesis results of Cu-NPs/*A.s* by plant aqueous extract were successfully carried out. A color change from the plant's extract dark brown to yellow on addition of the metal precursor (aqueous salt solution) indicated a reduction from Cu^{+2} to form Cu-NP/*A.s* (Fig. 2). This indicates that a redox reaction occurred between the metal salt and the active compounds in the aqueous plant extract, resulting in the formation of Cu-NPs [35]. The nucleation and growth of Cu-NPs are a direct result of the biomolecules in the aqueous extract solution behaving as reducing agents (*A.s* extracts).

Fig. 3 shows the UV-Vis spectra of *A.s* extract (ext.), which exhibits a wide peak around 372 nm. The appearance of the color is a strong indication of the presence of Cu-NP. It is thought that the position of the λ_{max} for Cu-NPs/*A.s* indicates the particle size. Other studies have observed maximum absorbances between 260 and 380 nm [34].

The FTIR spectrum of *A.s* extract shows several intense peaks (Fig. 4). A broad and prominent

a **b** **c**

Fig. 2: Clear solution of: A) Cu ions, B) *A.s* extract alone and C) Biosynthesized Cu-NPs/*A.s.*

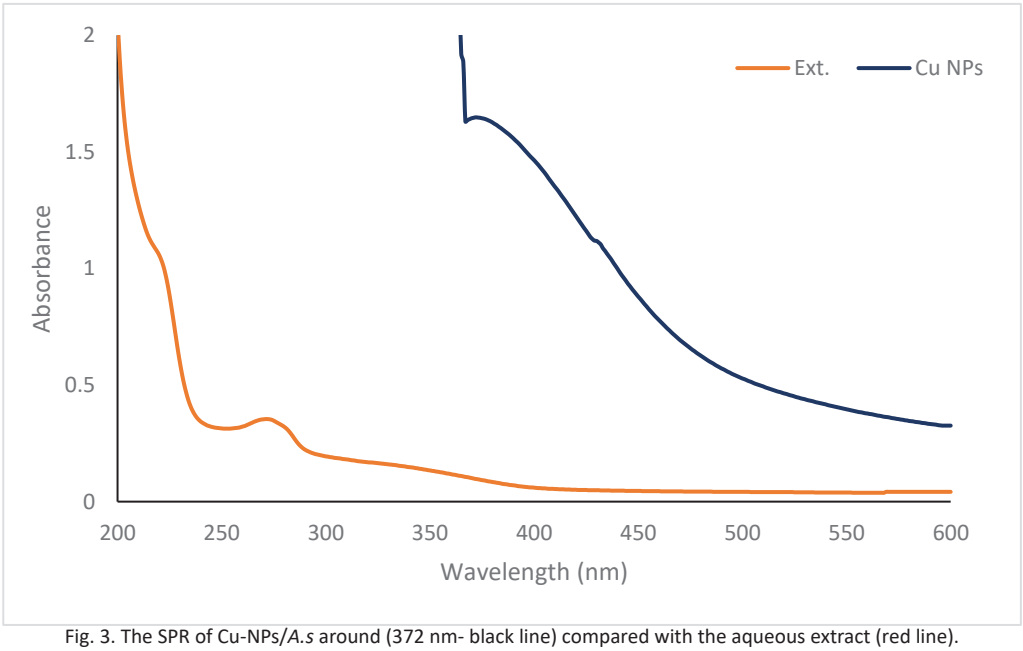

Fig. 3. The SPR of Cu-NPs/*A.s* around (372 nm- black line) compared with the aqueous extract (red line).

peak observed at 3414 cm^{-1} relates to the O–H stretching (attributable to alcohols, phenols, and flavones) [36]. The peak at 2939 cm^{-1} indicates C–H (aliphatic) stretching. The absorbance at 1639 cm^{-1} is related to the carbonyl group present in the ester complex of the extract. The peak at 1369 cm^{-1} could be attributed to the C–O bond. The absorption at 1200–900 cm^{-1} may indicate the C–O–C bands. According to these findings, the bioconversion of copper ions to copper nanoparticles may have been due to contributions by common functional groups of biomolecules found in the plant extract, including phenols, carbonyls, and aliphatic amines. It is thought that the disappearance of these functional groups after the synthesis of Cu-NPs/*A.s* can be interpreted as the pivotal role they play in Cu ions reduction [37].

The average particle size of Cu-NPs/*A.s* was measured by dynamic light scattering (DLS). (Fig. 5A) shows that the size of the particles was 18-76 nm and the polydispersity index (PdI) value was 0.324. The stability of Cu-NPs/*A.s* was investigated using the zeta potential (ζ), and the value was recorded as –25.2 mV, indicating moderate stability of the colloidal suspension. This provides the necessary minimum electrostatic repulsion while the layer of biomolecules and macromolecules from the *A.s* acts as a thick, physical barrier against aggregation [38]. This steric hindrance is the dominant factor preventing particle contact, particularly in high-ionic-strength environments such as biological media, where the electrostatic double layer is compressed and the strict ± 30 mV threshold is no longer the critical determinant of

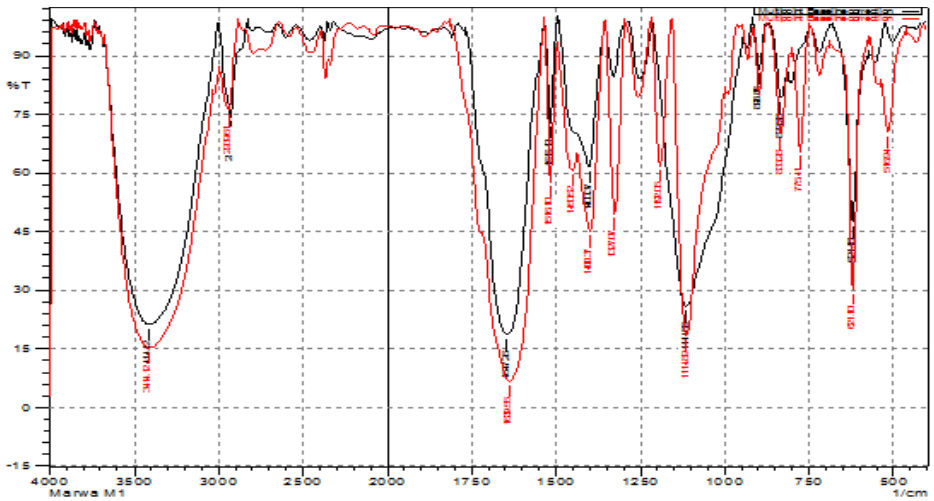

Fig. 4. FTIR spectra of biosynthesised Cu-NPs/*A.s*: the red curve represents aqueous *A.s* extract, and the black curve is Cu-NPs/*A.s*.

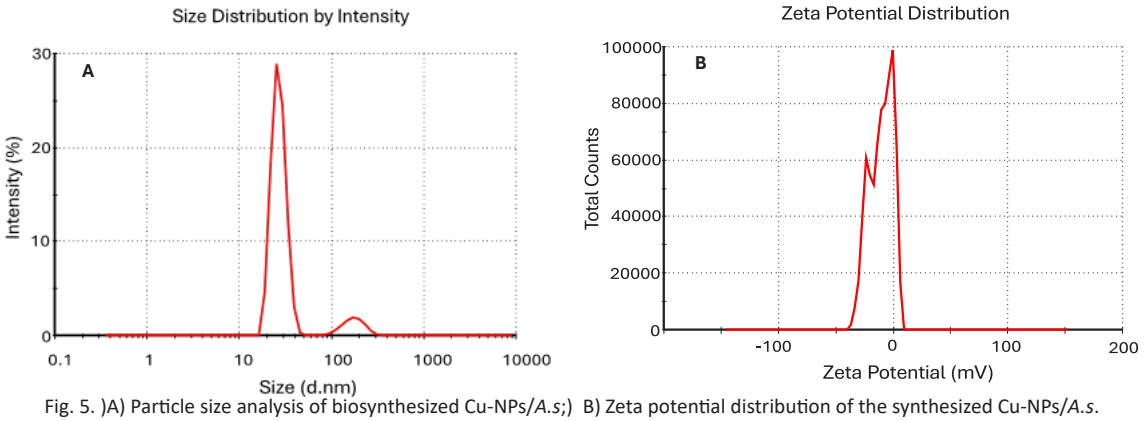

Fig. 5.)A) Particle size analysis of biosynthesized Cu-NPs/*A.s*;) B) Zeta potential distribution of the synthesized Cu-NPs/*A.s*.

stability.

Fig. 5B shows that the synthesized Cu-NPs/*A.s* were stable, as evidenced by the larger negative zeta potential value, which indicates that there is a low propensity for aggregation in the colloidal suspension of these biosynthesized nanoparticles [38]

Fig. 6 illustrates the stoichiometry of Cu-NPs/*A.s* and displays the chemical composition. The elemental analysis reveals the presence of the Cu element with a concentration of 9.13 wt%. Additional minor elements (C, N, O, Na) are present due to the presence of *A.s*. extract molecules.

Fig. 7 illustrates the morphology and the corresponding particle size of the CuNPs/*A.s* obtained by TEM. The mean diameter of Cu-NPs/*A.s* was measured at 63.7 ±19.5 nm. Most of the particles exhibit semi-spherical shapes with some aggregations. The slight differences in the particle size values reported by DLS and TEM are thought to be due to the inherent differences in the techniques. While DLS typically quantifies the hydrodynamic diameter of nanoparticles, which includes the core size and the diffuse layer surrounding it, TEM specifically measures the particle's core size. Consequently, nanoparticle sizes determined by DLS typically appear larger compared to those measured by TEM [39].

Phosphomolybdenum was used to investigate the antioxidant scavenging activity of the synthesized nanoparticles. This assay depends on the potential of Cu-NPs/*A.s* to reduce phosphate molybdenum (vi) to (v), producing a green color in the process of forming the phosphomolybdenum

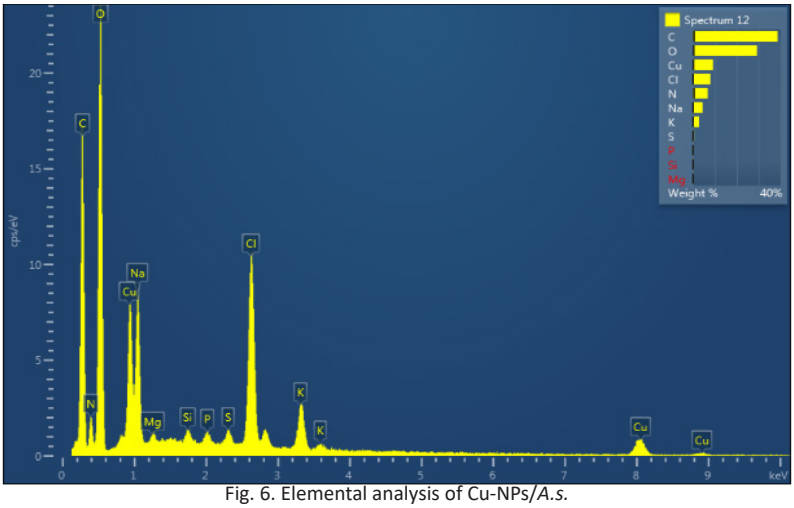

Fig. 6. Elemental analysis of Cu-NPs/*A.s.*

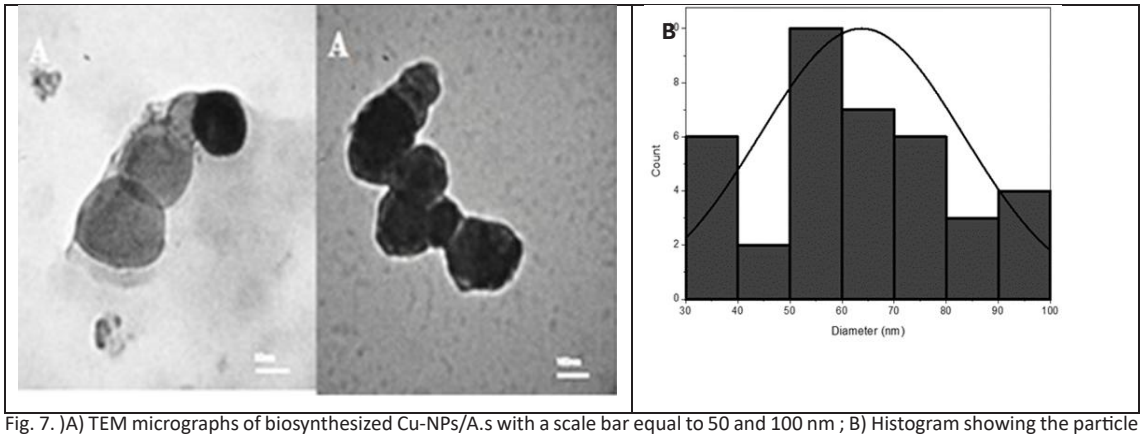

Fig. 7.)A) TEM micrographs of biosynthesized Cu-NPs/A.s with a scale bar equal to 50 and 100 nm ; B) Histogram showing the particle size distribution of Cu-NPs/*A.s*.

(v) complex. (Fig. 8) shows that the highest scavenging values of the Cu-NPs/*A.s* was 55 % ± 0.95, while ascorbic acid reached 76.35% at its highest tested concentration. The IC_{50} value for ascorbic acid was calculated as 27.65 µg/mL, representing the concentration required to achieve 50% scavenging [40].

The effect of Cu-NPs/*A.s* was evaluated on cells of MDCK-SIAT1 infected with IAV. The concentrations used were: 6.0, 12.0, 18.0, 24.0, and 32.0 µg/mL using cells pre-treated for 1.0 h (in triplicate). The IAV particles were eliminated using neutralizing antibodies, and the virus was quantified by neuraminidase activity analysis. (Fig. 9) shows the antiviral activity of Cu-NPs/*A.s* with the IAV. The findings demonstrate that the antiviral activity increased with increasing total concentrations of Cu-NPs/*A.s.* The highest Neuraminidase inhibition rates are 70.67 % at 32.0 µg/mL, and similarly, all concentrations showed good activity. This confirms the key role of *A.s* bio-substances incorporated into the Cu-NPs in enhancing antiviral activity against IAV and reducing cytotoxicity in MDCK-SIAT1 cells. The results displayed good agreement with findings from several other studies [41]. The mechanism of antiviral effect for Cu-NPs/*A.s* against the IAV may involve the interactions between the Cu nanostructures and the viral surface glycoproteins, such as hemagglutinin and neuraminidase. Cu-NPs/*A.s* may bind to the surface of the virus through glycoproteins and then enter their cells [42]. Further, it is thought

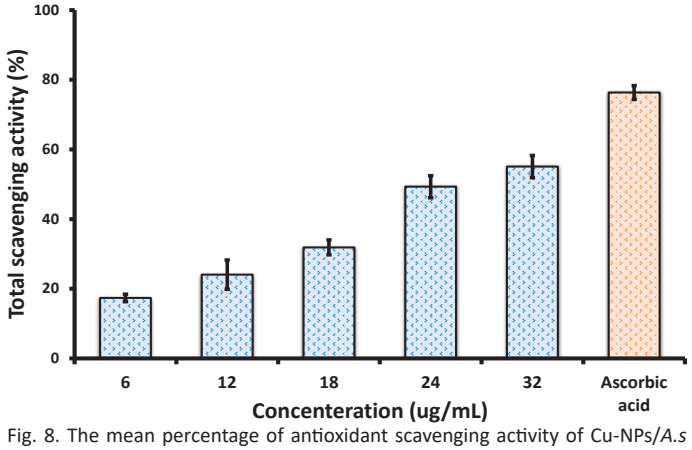

Fig. 8. The mean percentage of antioxidant scavenging activity of Cu-NPs/*A.s* compared with standard ascorbic acid (mean ± SD, n=3).

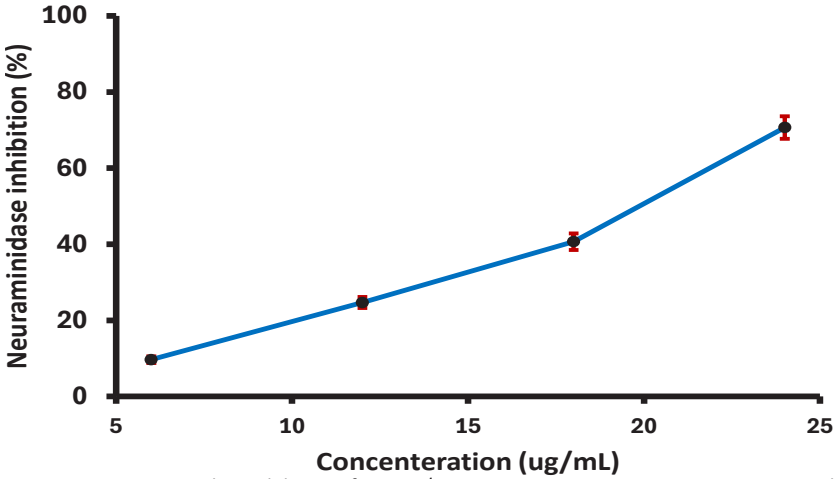

Fig. 9. Mean neuraminidase inhibition of Cu-NPs/*A.s* at concentrations 6.0, 12.0, 18.0, 24.0, and 32.0 µg/mL (mean ± SD, n=3).

that these antiviral mechanisms manifest in a similar way as seen in Cu oxides against hepatitis C and the herpes simplex viruses, and influenza viruses. So, aside from preventing viral entry and attachment to the host cells through interactions with the surface of glycoproteins [43]. Another pathway that could be exhibited by Cu-NPs/*A.s* is in impairing viral replication. This could be through interacting with the virus's genetic material and hindering its propagation, which could be useful in the fight against SARS-CoV. Additionally, these Cu-NPs/*A.s* could induce the formation of reactive oxygen species (ROS), which could contribute to viral inactivation by degrading viral proteins and

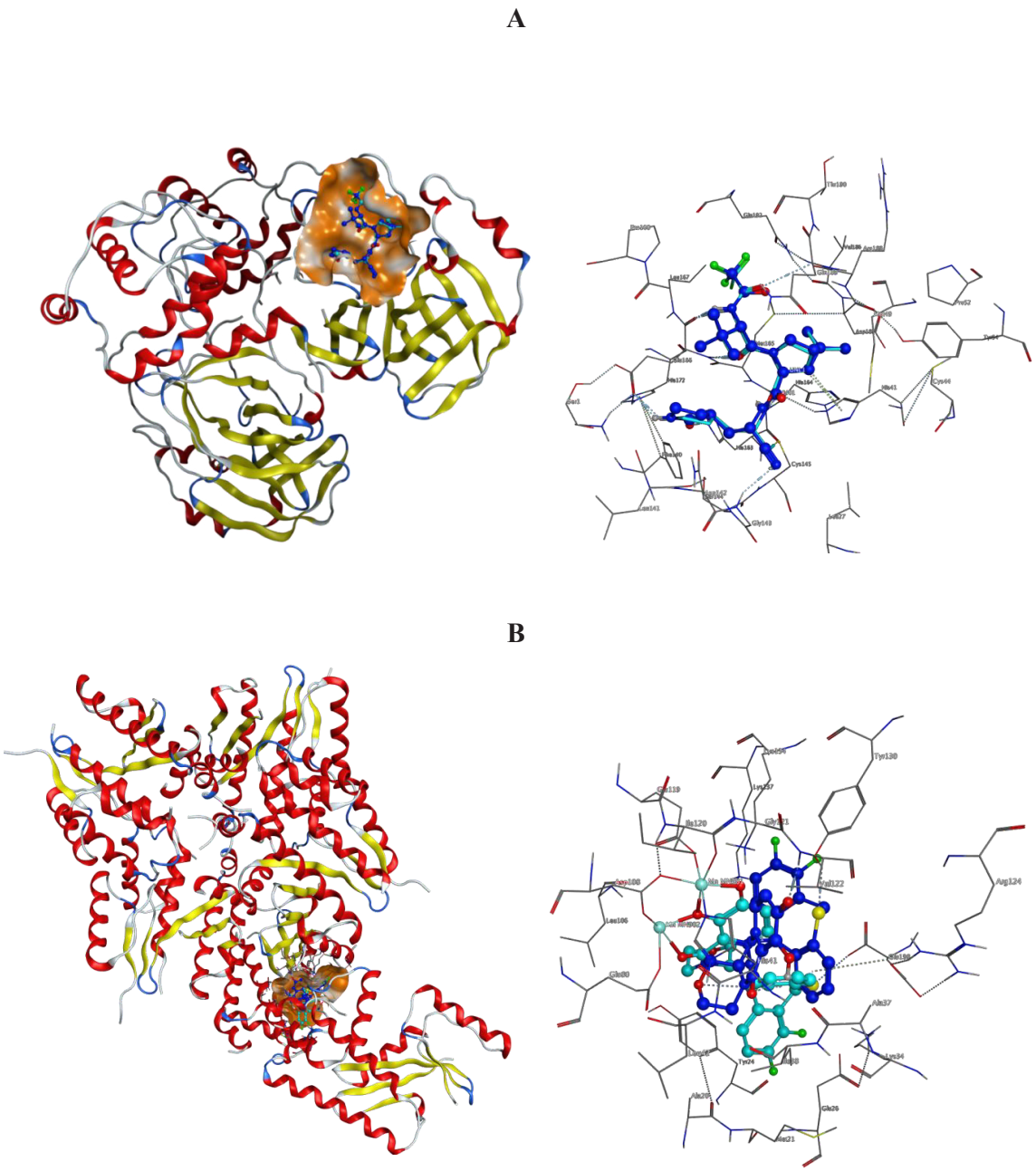

Fig. 10. (A) Superposition models of Nirmatrelvir (6) bound to SARS-CoV-2 (PDB ID: 8DZ2) and the proposed binding conformation obtained from the docking simulation (B) superposition models of Baloxavir bound to influenza A virus RNA polymerase (PDB ID: 6FS6) and the proposed binding conformation obtained from the docking simulation.

nucleic acids [44,45].

The molecular docking study was conducted using the Molecular Operating Environment (MOE) software (Inc, 2019), which examined the binding mode, binding conformation, and affinities of the synthesized compounds with SARS-CoV-2 (PDB ID: 8DZ2) and influenza A virus RNA polymerase (PDB ID: 6FS6). To validate our molecular approach and

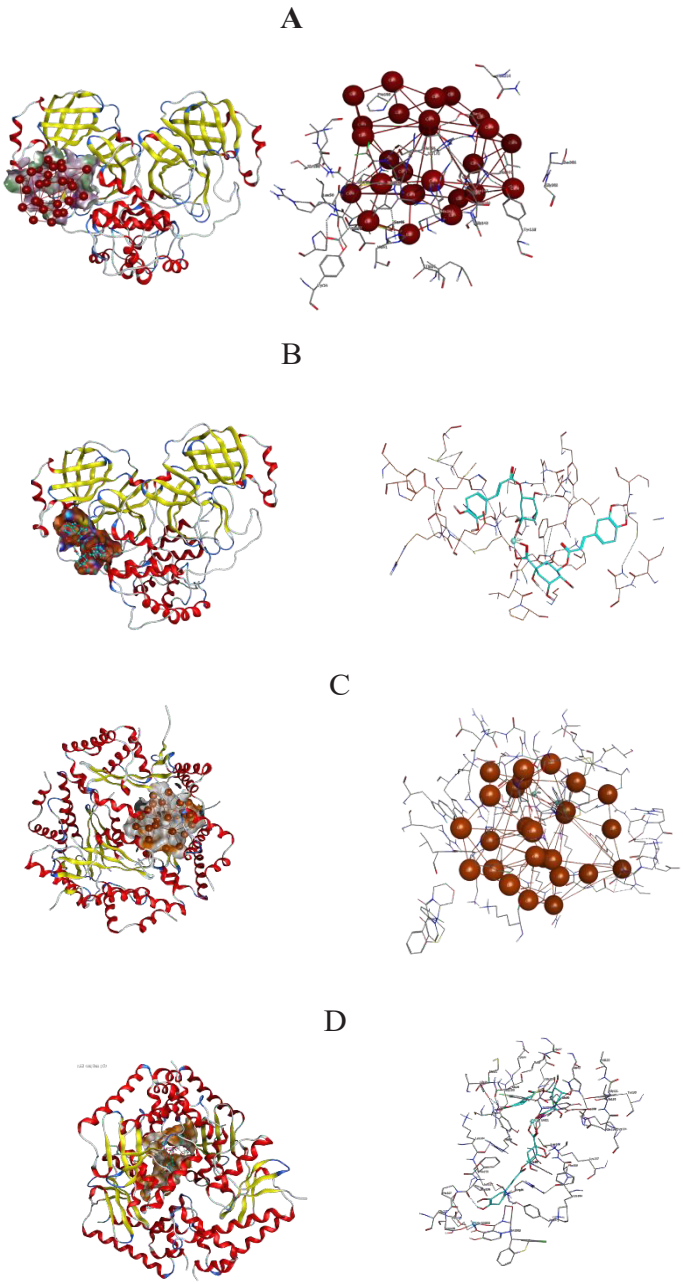

Fig. 11. Docked models of the synthesised compounds (a) Estimated binding conformation of the compound Cu-NPs /*A.s* bound to main protease of SARS-CoV-2 (PDB ID: 8DZ2) (b) Estimated binding conformation of the compound CGA-Cu NPs /*A.s* bound to main protease of SARS-CoV-2 (PDB ID: 8DZ2) (c) Estimated binding conformation of the Cu-NPs /*A.s* bound to influenza A virus RNA polymerase (PDB ID: 6FS6) (d) Estimated binding conformation of the CGA-Cu NPs /*A.s* influenza A virus RNA polymerase (PDB ID: 6FS6).

verify MOE's capability to accurately represent the orientation and position of the native ligands in the crystal structures, we redocked the co-crystal standard ligands Nirmatrelvir and Baloxavir as reference compounds. The simulations successfully produced valid putative binding modes with energy scores of −10.02 kcal/mol for Nirmatrelvir bound to SARS-CoV-2 (PDB ID: 8DZ2) and −9.63 kcal/mol for Baloxavir bound to influenza A virus RNA polymerase. The root mean square deviations (RMSDs) between the docked conformation and the co-crystallized ligands were determined to be 1.97 for SARS-CoV-2 and 1.82 for influenza A virus RNA polymerase. Fig.

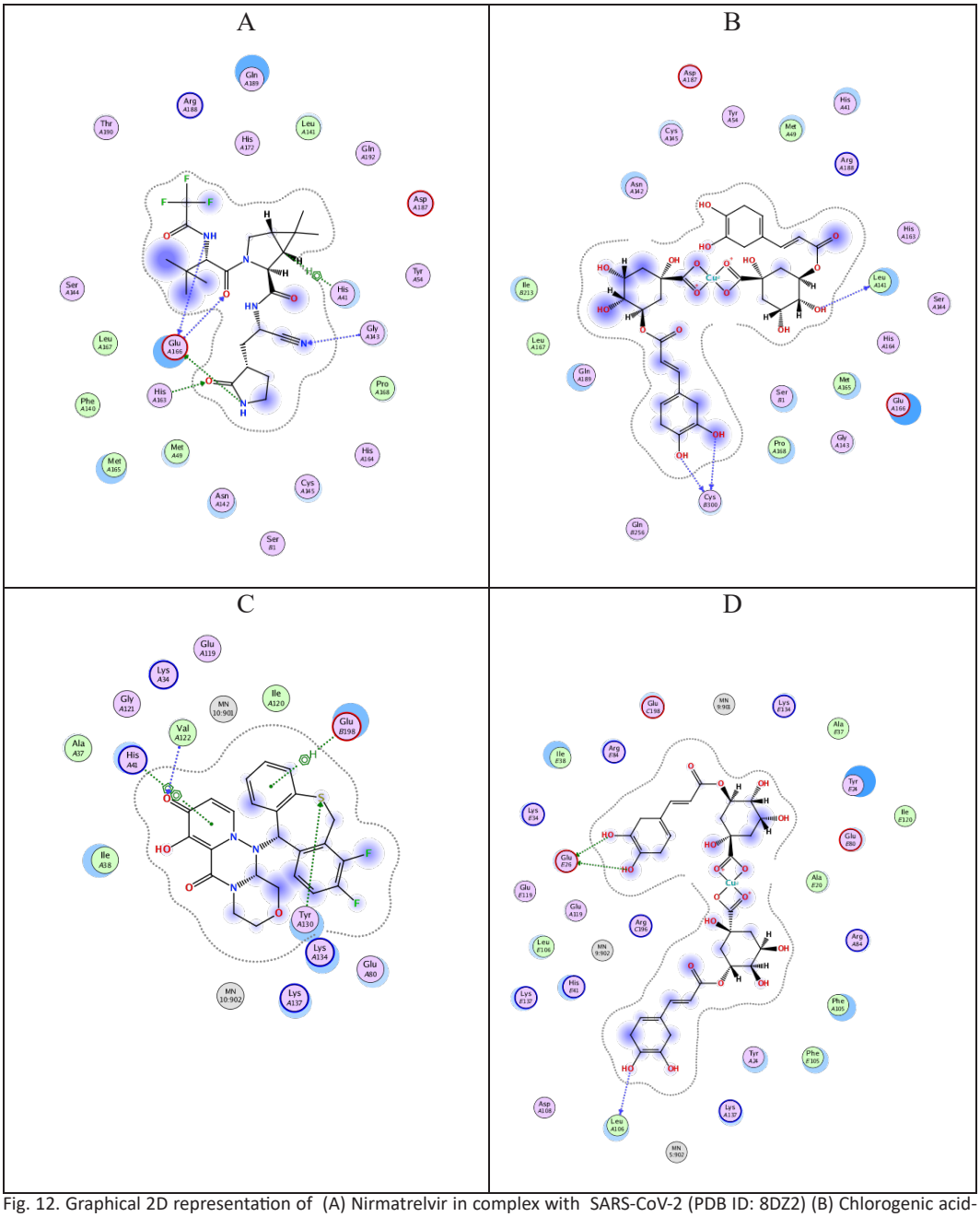

Fig. 12. Graphical 2D representation of (A) Nirmatrelvir in complex with SARS-CoV-2 (PDB ID: 8DZ2) (B) Chlorogenic acid-Cu-NPs/*A.s* in complex with SARS-CoV-2 (PDB ID: 8DZ2) (C) Baloxavir bound to influenza A virus RNA polymerase (PDB ID: 6FS6) (D) Chlorogenic acid- Cu-NPs/*A.s* in complex with influenza A virus RNA polymerase (PDB ID: 6FS6).

10 depicts the conformational superpositions of Nirmatrelvir and Baloxavir obtained from the X-ray crystal structures, alongside Nirmatrelvir and Baloxavir obtained from the docking simulations. The estimated binding modes of the docked Nirmatrelvir and Baloxavir were similar in both pockets.

Once the validity of the docking methodology was confirmed for the molecular docking investigation, the individually synthesized molecules were docked with SARS-CoV-2 and influenza A virus RNA polymerase using the same criteria employed during validation. We performed 5 docking iterations for each ligand, choosing the best-scoring configuration of each ligand-enzyme complex according to energy parameters and RMSD values. Figs. 10 and 11 illustrate the best-scoring poses of Cu-NPs /*A.s* and CGA-Cu NPs compounds from the docking studies, alongside the essential residues within the binding site. The predicted RMSDs and binding free energies obtained from molecular experiments are shown in Table 1. The complex CGA-Cu NPs /*A.s* achieved a favourable binding affinity of −8.22 kcal/mol and -9.04 for the SARS-CoV-2 main protease and influenza A virus RNA polymerase 2, respectively. The presence of Cu-NPs may influence the nature and strength of these interactions. These docking results highlight the potential of chlorogenic acid–Cu-NPs as antiviral candidates against SARS-CoV-2 [46]. The interactions are primarily driven by electrostatic forces and Van der Waals interactions, which are critical for stabilizing the ligand–protein complex [47]. This data provides valuable insights for computational studies aimed at understanding the binding mechanisms of chlorogenic acid and its nanoparticle conjugates during antiviral drug development.

Quantum Chemical Calculation Results

Based on the results of the DFT computation, the optimized Cu-complex is shown in Fig. 13. It was noted that an energy value of −2789.75 Hartree, showing that the Cu-complex is quite stable thermodynamically. Based on the frontier molecular orbital calculation, the energy values of HOMO and LUMO were identified to be −0.35859 Hartree and −0.34511 Hartree, which convert to −9.7221 eV and −9.3566 eV, respectively.

The energy gap between HOMO and LUMO was computed to be 0.3655 eV, showing a relatively small value and therefore implying that the Cu-complex is more chemically reactive, has high polarizability, and good charge transfer ability

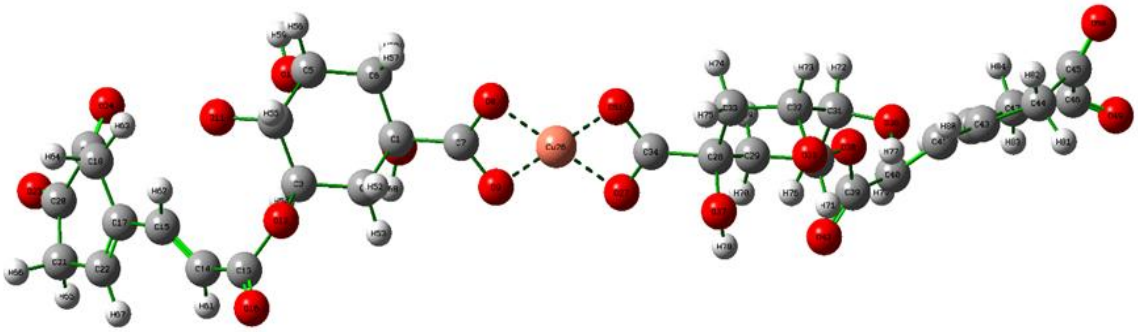

Fig. 13. Optimized structure of Cu-NPs/*A.s*.

Table 1. Binding scores RMSD- refine values of the investigated compounds.

Compound ID	Main protease of SARS-CoV-2		Influenza A virus RNA polymerase	
	Binding Energy kcal/mol	RMSD- refine	Binding Energy kcal/mol	RMSD- refine
Nirmatrelvir	-8.9021	1.9762	-	-
Baloxavir	-	-	-5.5577	1.8226
Cu-NPs /*A.s*	-0.8675	6.5285	-0.2400	6.5073
CGA-Cu NPs /*A.s*	-8.2268	1.8906	-9.0401	2.0098

within itself. Compounds with lower band gap values usually show better electronic transitions and are able to interact better with their surroundings, as shown in Figs. 13 and 14.

The ionization energy of the complex (9.7221 eV) shows that a large amount of energy is needed to extract an electron from the molecule, which implies good stability of the complex on the electronic level. Similarly, a high value of electron affinity (9.3566 eV) reflects the high capacity of the molecule for accepting electrons.

The value of chemical softness (0.0524) shows that the Cu-complex has a considerable degree of polarizability and can be used effectively for intermolecular interaction and charge transfer processes. The negative value of chemical potential (−0.1827) further supports the thermodynamic stability of the compound. Moreover, the positive value of electrophilicity index (0.00175) shows electrophilic nature of the complex, as shown in

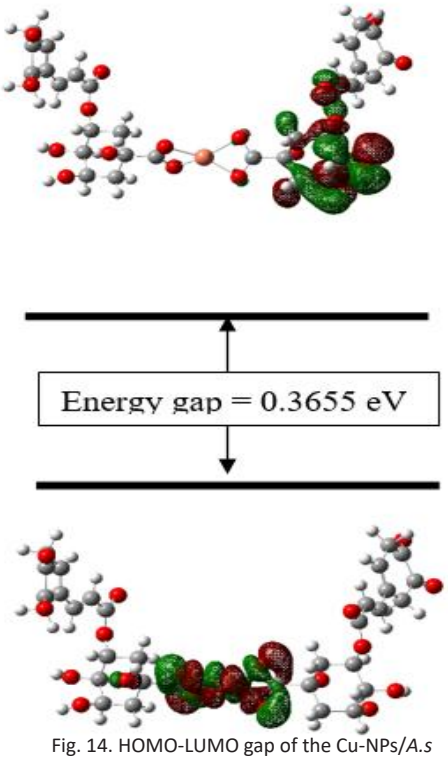

Fig. 14. HOMO-LUMO gap of the Cu-NPs/*A.s*

Table 2. Global reactivity descriptors of selected complex.

Parameter	Value
Total Energy (Hartree)	−2789.75
HOMO (Hartree)	−0.35859
LUMO (Hartree)	−0.34511
HOMO (eV)	−9.7221
LUMO (eV)	−9.3566
Ionization Potential (IP)	9.7221 eV
Electron Affinity (EA)	9.3566 eV
Energy Gap (ΔE)	0.3655 eV
Chemical Hardness (η)	9.5394
Chemical Softness (S)	0.0524
Chemical Potential (μ)	−0.1827
Electronegativity (χ)	0.1827
Electrophilicity Index (ω)	0.00175

Table 2.

Frontier Molecular Orbital (FMO) Distribution

The diagram below shows the distribution of frontier molecular orbitals of the Cu-complex from the DFT calculations. The green color shows the electron distribution density of the molecular orbital, which gives valuable insight into the electronic characteristics and charge transfer abilities of the complex.

The orbital density is mostly concentrated in the vicinity of the copper center along with the surrounding conjugated ligands, meaning there is effective electronic communication between the metal and ligand parts of the complex. The high degree of delocalization ensures efficient intramolecular charge transfer, which boosts the chemical stability and reactivity of the complex, as shown in Fig. 15.

The presence of an electron cloud in the coordination sphere means the contribution of the Cu atom to the frontier molecular orbitals, improving the electron movement and facilitating the donor-acceptor interactions inside the molecule. The delocalization of the orbitals also accounts for the small energy difference between the HOMO and LUMO states from the DFT calculations.

The considerable overlap of orbitals between the metal center and the ligands suggests effective hybridization and conjugation of the complex, likely increasing the catalytic activity, electrical conductivity, and biological interaction ability of the complex.

The ProTox-3.0

Table 3 shows the expected results using ProTox-3.0 are characteristic of the combined hearing aid. The most interesting finding was the recorded immunotoxicity rating (IMP) with a very high probability of 0.99, the highest value. This indicates that the compound is likely to contribute to the development, success, or abnormal facilitation of adverse organ reactions, such as allergic reactions. This characteristic makes it possible for many chemical or agricultural agents to be recorded without proper verification.

Another notable finding was that the compound exhibited activity in the Blood-brain barrier (BBB) with a probability of 0.64. This means that the compound is capable of reaching the central nervous system, which could lead to undesirable central nervous system effects, even though the neurotoxicity rating was inactive (0.91). It is possible for the compound to cause neurological or cognitive effects without being neurotoxic.

Regarding organo-toxicity, the compound was non-hepatotoxic (0.69), non-neurotoxic (0.91), and non-cardiotoxic (0.88), which are reassuring results. However, it showed weak activity for both specific (0.53) and respiratory (0.54) toxicity. While these possibilities are low, they cannot

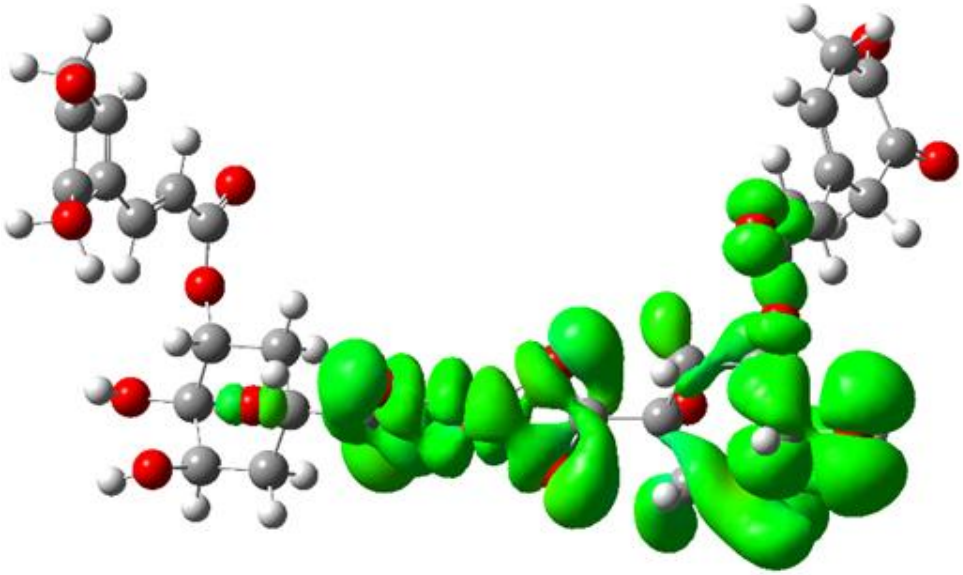

Fig. 15. FMO distribution of complex Cu-NPs/*A.s.*

be disregarded, especially if the compound is administered at high doses or for extended periods.

Another important point is that all tissue stress pathways (HSE, MMP, p53, ATAD5) are not high-probability devices (0.82–0.91), indicating that the compound does not induce oxidative stress, mitochondrial kinase, or high-variability p53 synthesis, which are important components of many toxic compounds. This suggests that the main target pathway for the compound is available but not directly exclusive.

The compound exhibited a faster-acting THRα (Thyroid-first-age aging) potential of 0.81, suggesting possible interference with the photosystems, particularly the regulation of glandular maturation. This vulnerability, however slight, may be significant in chronic disease cases.

Furthermore, all tested CYP450 enzymes were non-robots toward the compound, with very high probabilities (up to 0.99 for CYP2E1). This indicates that the compound is virtually invisible to these enzymes, potentially leading to minimal excretion from the body, only plasma concentrations, and a long half-life. It also suggests that it is less likely to be involved in drug interactions based on the benefits or induction of these enzymes. The toxicity results for LD_{50} as reported in the software Pro Tox-3.0.

The possibility of approving the compound as

Table 3. ProTox-3.0 - Prediction of toxicity of chemicals.

Classification	Target	Shorthand	Prediction	Probability
Organ toxicity	Hepatotoxicity	dili	Inactive	0.69
Organ toxicity	Neurotoxicity	neuro	Inactive	0.91
Organ toxicity	Nephrotoxicity	nephro	Active	0.53
Organ toxicity	Respiratory toxicity	respi	Active	0.54
Organ toxicity	Cardiotoxicity	cardio	Inactive	0.88
Toxicity endpoints	Carcinogenicity	carcino	Inactive	0.74
Toxicity endpoints	Immunotoxicity	immuno	Active	0.99
Toxicity endpoints	Mutagenicity	mutagen	Inactive	0.79
Toxicity endpoints	Cytotoxicity	cyto	Inactive	0.80
Toxicity endpoints	BBB-barrier	bbb	Active	0.64
Toxicity endpoints	Clinical toxicity	clinical	Active	0.66
Toxicity endpoints	Nutritional toxicity	nutri	Inactive	0.62
Tox21-Stress response pathways	Heat shock factor response element (HSE)	sr_hse	Inactive	0.82
Tox21-Stress response pathways	Mitochondrial Membrane Potential (MMP)	sr_mmp	Inactive	0.90
Tox21-Stress response pathways	Phosphoprotein (Tumor Suppressor) p53	sr_p53	Inactive	0.91
Tox21-Stress response pathways	ATPase family AAA domain-containing protein 5 (ATAD5)	sr_atad5	Inactive	0.91
Molecular Initiating Events	Thyroid hormone receptor alpha (THRα)	mie_thr_alpha	inActive	0.81
Molecular Initiating Events	Thyroid hormone receptor beta (THRβ)	mie_thr_beta	Inactive	0.92
Metabolism	Cytochrome CYP1A2	CYP1A2	Inactive	0.94
Metabolism	Cytochrome CYP2C19	CYP2C19	Inactive	0.95
Metabolism	Cytochrome CYP2C9	CYP2C9	Inactive	0.55
Metabolism	Cytochrome CYP2D6	CYP2D6	Inactive	0.86
Metabolism	Cytochrome CYP3A4	CYP3A4	Inactive	0.97
Metabolism	Cytochrome CYP2E1	CYP2E1	Inactive	0.99

Table 4. The potential for pharmaceutical development (Positives).

Property	Result	Comment
Hepatotoxicity	Inactive (0.69)	Relatively safe for the liver
Cardiotoxicity	Inactive (0.88)	Relatively safe for the heart
Neurotoxicity	Inactive (0.91)	Relatively safe for the nerves
Mutagenicity	Inactive (0.79)	Does not cause genetic mutations
Carcinogenicity	Inactive (0.74)	Does not cause cancer
Cytotoxicity	Inactive (0.80)	Does not directly kill cells
p53 pathway	Inactive (0.91)	Does not activate tumor suppression response

a medicine depends on the program results, as shown in the Table 4.

These results are very encouraging from the perspective of basic pharmaceutical safety, as most drugs that fail do so due to hepatotoxicity, cardiotoxicity, or mutagenicity.

CONCLUSION

A green chemistry approach was attempted to synthesize Cu-NPs using *Artemisia sieberi.* The extract is thought to act as a reducing and capping agent, which are necessary in the biosynthesis of Cu-NPs/*A.s*. FTIR study revealed that their reduction by the extract was facilitated through reactive bio-functional groups, which play a key role in ion chelation and reduction. The findings demonstrated that Cu-NPs/*A.s* possess good antioxidant properties, exhibiting a good scavenging value compared with that of ascorbic acid. The synthesised nanoparticles also displayed antiviral activity against influenza A virus, as seen in the high neuraminidase inhibition rates. The positive molecular docking result further supports their potential applications, suggesting that Cu-NPs/*A.s* and related derivatives may be valuable in combating SARS-CoV-2.

All DFT parameters reflect good electronic characteristics, charge transfer capacity, and high reactivity of the Cu-NPs/*A.s.* It could be considered a potential drug candidate for very limited therapeutic purposes, such as immunosuppression in severe autoimmune diseases or organ transplantation, provided that extensive immunotoxicity studies are conducted and the benefit-risk assessment is carefully evaluated. However, for non-pharmaceutical applications (such as pesticides or industrial chemicals), extreme caution should be exercised due to its ability to cross the blood-brain barrier and induce immunomodulatory effects.

Therefore, the exploration of aqueous Cu-NPs/*A.s* formulations (*in vitro and in vivo*) as antiviral agents for SARS-CoV-2 treatment may be recommended in future pandemics as a new nanomedicine-centered approach, one that combines advantages offered by nanoscale materials to treat disease and enhance life. Further, adopting a new nanomedicine-based strategy that incorporates the special benefits of nanoscale materials to treat illness and enhance quality of life may lead to the recommendation of formulations (proven in vitro and in vivo) as antiviral medicines against SARS-CoV-2 in future pandemics.

CONFLICT OF INTEREST

The authors declare that there is no conflict of interests regarding the publication of this

manuscript.

REFERENCES

1. Tomaszewska E, Bednarczyk K, Janicka M, Chodkowski M, Krzyzowska M, Celichowski G, et al. The Influence of the AgNPs Ligand on the Antiviral Activity Against HSV-2. International Journal of Nanomedicine. 2025;Volume 20:2659-2671.
2. Ullah R, Siraj M, Zarshan F, Abbasi BA, Yaseen T, Waris A, et al. A comprehensive overview of fabrication of biogenic multifunctional metal/metal oxide nanoparticles and applications. Reviews in Inorganic Chemistry. 2024;45(2):411-436.
3. Arshad F, Naikoo GA, Hassan IU, Chava SR, El-Tanani M, Aljabali AA, et al. Bioinspired and Green Synthesis of Silver Nanoparticles for Medical Applications: A Green Perspective. Applied Biochemistry and Biotechnology. 2023;196(6):3636-3669.
4. Kundu S, Kues WA, Rehbock C, Barcikowski S. Inorganic Metal Nanoparticles in Reproductive Biology: Applications, Toxicities and Future Prospects. ChemPlusChem. 2025;90(5)..
5. Dharmalingam Jothinathan MK, Behera A, Ramalingam S, Alam MM, Amanullah M, Karunakaran R. Review on bio-selenium nanoparticles: Synthesis, protocols, and applications in biomedical processes. Nanotechnology Reviews. 2025;14(1)..
6. Bidan AK, Al-Ali ZSA. Biomedical Evaluation of Biosynthesized Silver Nanoparticles by Jasminum Sambac (L.) Aiton Against Breast Cancer Cell Line, and Both Bacterial Strains Colonies. International Journal of Nanoscience. 2022;21(06)..
7. Bairwa P, Devra V. Plant-mediated bimetallic nanoparticles synthesis for catalytic degradation of malachite green. Academia Engineering. 2024;1(3)..
8. Majeed S, Iman AJA-T, Abdullah HA-S. Enhancing Antifungal Property And Cytotoxicity Profile Of Gold Nanoparticles Biosynthesis Via Some Filamentous Fungi With In Silico Study. Journal of Medical Genetics and Clinical Biology. 2025;2(5):201-221.
9. Jaffer Al-Timimi IA, Sermon PA, Burghal AA, Salih AA, Alrubaya IMN. Nanoengineering the antibacterial activity of biosynthesized nanoparticles of TiO_2, Ag, and Au and their nanohybrids with Portobello mushroom spore (PMS) (TiO_x/PMS, Ag/PMS and Au/PMS) and making them optically self-indicating. SPIE Proceedings; 2016/09/27: SPIE; 2016. p. 99300B.
10. Roy N, T N, Paira P, Chakrabarty R. Selenium-based nanomaterials: green and conventional synthesis methods, applications, and advances in dye degradation. RSC Advances. 2025;15(4):3008-3025.
11. Hashem AH, Al-Askar AA, Haponiuk J, Abd-Elsalam KA, Hasanin MS. Biosynthesis, Characterization, and Antifungal Activity of Novel Trimetallic Copper Oxide–Selenium–Zinc Oxide Nanoparticles against Some Mucorales Fungi. Microorganisms. 2023;11(6):1380.
12. Pourmadadi M, Holghoomi R, shamsabadipour A, Maleki-baladi R, Rahdar A, Pandey S. Copper nanoparticles from chemical, physical, and green synthesis to medicinal application: A review. Plant Nano Biology. 2024;8:100070.
13. Zayed MA, Abdel-Aziz HM, Abdel-Gawad SA. Adsorptive removal of reactive yellow S3R dye from aqueous solutions using green-synthesized copper nanoparticles. Sci Rep. 2026;16(1)..
14. Rahman G, Fazal H, Ullah A, Ahmad S, Nadeem T, Ahmad M, et al. Empowering silver and copper nanoparticles through aqueous fruit extract of Solanum xanthocarpum for sustainable advancements. Biomass Conversion and Biorefinery. 2024;15(4):5155-5169.
15. Pourmadadi M, Ghaemi A, Shamsabadipour A, Rajabzadeh-Khosroshahi M, Shaghaghi M, Rahdar A, et al. Nanoparticles loaded with Daunorubicin as an advanced tool for cancer therapy. Eur J Med Chem. 2023;258:115547.
16. Khan SK, Dutta J, Rather MA, Ahmad I, Nazir J, Shah S, et al. Assessing the Combined Toxicity of Silver and Copper Nanoparticles in Rainbow Trout (Oncorhynchus mykiss) Fingerlings. Biol Trace Elem Res. 2025;203(11):5838-5856.
17. Hamouda RA, Aljohani ES. Assessment of Silver Nanoparticles Derived from Brown Algae Sargassum vulgare: Insight into Antioxidants, Anticancer, Antibacterial and Hepatoprotective Effect. Mar Drugs. 2024;22(4):154.
18. Villagrán Z, Anaya-Esparza LM, Velázquez-Carriles CA, Silva-Jara JM, Ruvalcaba-Gómez JM, Aurora-Vigo EF, et al. Plant-Based Extracts as Reducing, Capping, and Stabilizing Agents for the Green Synthesis of Inorganic Nanoparticles. Resources. 2024;13(6):70.
19. Iawal H, Saeed SI, Gaddafi MS, Kamaruzzaman NF. Green Nanotechnology: Naturally Sourced Nanoparticles as Antibiofilm and Antivirulence Agents Against Infectious Diseases. Int J Microbiol. 2025;2025(1).
20. Bilal M, Bandyopadhyay S. Controlled growth of citrate-stabilized gold nanoparticles using a semi-continuous seed-mediated route. Discover Nano. 2025;20(1).
21. Murthy HCA, Desalegn T, Kassa M, Abebe B, Assefa T. Synthesis of Green Copper Nanoparticles Using Medicinal Plant Hagenia abyssinica (Brace) JF. Gmel. Leaf Extract: Antimicrobial Properties. Journal of Nanomaterials. 2020;2020:1-12.
22. Al-Otibi F, Alshammry NA, Alharbi RI, Bin-Jumah MN, AlSubaie MM. Silver Nanoparticles of Artemisia sieberi Extracts: Chemical Composition and Antimicrobial Activities. Plants. 2023;12(11):2093.
23. Copper Leachability from Cu Nanoparticle-Containing Face Masks and Associated Subcellular Impacts. American Chemical Society (ACS). http://dx.doi.org/10.1021/acs.estlett.2c00954.s001
24. Yazdani Sani N, Akhlaghi H, Motavalizadehkakhky A. Bio-inspired synthesis of copper nanocatalysts using chlorogenic acid isolated from Prangos serpentinica for efficient aqueous-phase Henry reactions. Discover Nano. 2026;21(1).
25. Yu W, Tang J, Gao C, Zheng X, Zhu P. Green Synthesis of Copper Nanoparticles from the Aqueous Extract of Lonicera japonica Thunb and Evaluation of Its Catalytic Property and Cytotoxicity and Antimicrobial Activity. Nanomaterials. 2025;15(2):91.
26. Asmat-Campos D, Rojas-Jaimes J, de Oca-Vásquez GM, Nazario-Naveda R, Delfín-Narciso D, Juárez-Cortijo L, et al. Biogenic production of silver, zinc oxide, and cuprous oxide nanoparticles, and their impregnation into textiles with antiviral activity against SARS-CoV-2. Sci Rep. 2023;13(1).
27. Sergeeva Y, Yeung SY, Hix-Janssens T, Sellergren B. Gold Nanoparticles with Adaptable Self-Assembled Monolayer Shells Allow Multivalent Inhibition and Sensing of Influenza Virus at Ultralow Concentrations. ACS Central Science. 2025;11(9):1659-1669.
28. Mosidze E, Franci G, Dell'Annunziata F, Capuano N, Colella

M, Salzano F, et al. Silver Nanoparticle-Mediated Antiviral Efficacy against Enveloped Viruses: A Comprehensive Review. Global Challenges. 2025;9(5).
29. Ha T, Pham TTM, Kim M, Kim Y-H, Park J-H, Seo JH, et al. Antiviral Activities of High Energy E-Beam Induced Copper Nanoparticles against H1N1 Influenza Virus. Nanomaterials. 2022;12(2):268.
30. Argaman N, Makov G. Density functional theory: An introduction. Am J Phys. 2000;68(1):69-79.
31. Legge FS, Nyberg GL, Peel JB. DFT Calculations for Cu-, Ag-, and Au-Containing Molecules. The Journal of Physical Chemistry A. 2001;105(33):7905-7916.
32. Banerjee P, Kemmler E, Dunkel M, Preissner R. ProTox 3.0: a webserver for the prediction of toxicity of chemicals. Nucleic Acids Res. 2024;52(W1):W513-W520.
33. Asha TM, Prathapachandra Kurup MR. An insight into the potent antioxidant activity of a dithiocarbohydrazone appended cis-dioxidomolybdenum (VI) complexes. Appl Organomet Chem. 2020;34(9).
34. Salamanca A, Almodóvar P, Jarama I, González-Hedström D, Prodanov M, Inarejos-García AM. Anti-influenza virus activity of the elenolic acid rich olive leaf (Olea europaea L.) extract Isenolic. Antiviral Chem Chemother. 2021;29.
35. Pandey R, Vishwakarma V. Green synthesis of metal-based nanoparticles using Aloe vera (L.) Burm.f: A review. Discover Chemistry. 2026;3(1).
36. Amaliyah S, Pangesti DP, Masruri M, Sabarudin A, Sumitro SB. Green synthesis and characterization of copper nanoparticles using Piper retrofractum Vahl extract as bioreductor and capping agent. Heliyon. 2020;6(8):e04636.
37. Thejeswini PG, Nidhi MKJ, Giddaerappa, Reddy BU. Integrated Electrochemical and Biomedical Properties of Cu-Doped ZnO NPs Synthesized via Green Methods. ACS Omega. 2026;11(8):13160-13171.
38. Eid AM, Fouda A, Hassan SE-D, Hamza MF, Alharbi NK, Elkelish A, et al. Plant-Based Copper Oxide Nanoparticles; Biosynthesis, Characterization, Antibacterial Activity, Tanning Wastewater Treatment, and Heavy Metals Sorption. Catalysts. 2023;13(2):348.
39. Jassim AY, Wang J, Chung KW, Loosli F, Chanda A, Scott GI, et al. Comparative assessment of the fate and toxicity of chemically and biologically synthesized silver nanoparticles to juvenile clams. Colloids Surf B Biointerfaces. 2022;209:112173.
40. Bibi Sadeer N, Montesano D, Albrizio S, Zengin G, Mahomoodally MF. The Versatility of Antioxidant Assays in Food Science and Safety—Chemistry, Applications, Strengths, and Limitations. Antioxidants. 2020;9(8):709.
41. Cortes AA, Zuñiga JM. The use of copper to help prevent transmission of SARS-coronavirus and influenza viruses. A general review. Diagnostic Microbiology and Infectious Disease. 2020;98(4):115176.
42. Hadinejad F, Morad H, Jahanshahi M, Zarrabi A, Pazoki-Toroudi H, Mostafavi E. A Novel Vision of Reinforcing Nanofibrous Masks with Metal Nanoparticles: Antiviral Mechanisms Investigation. Advanced Fiber Materials. 2023;5(4):1273-1317.
43. Govind V, Bharadwaj S, Sai Ganesh MR, Vishnu J, Shankar KV, Shankar B, et al. Antiviral properties of copper and its alloys to inactivate covid-19 virus: a review. BioMetals. 2021;34(6):1217-1235.
44. Dehghani F, Mosleh-Shirazi S, Shafiee M, Kasaee SR, Amani AM. Antiviral and antioxidant properties of green synthesized gold nanoparticles using Glaucium flavum leaf extract. Applied Nanoscience. 2022;13(6):4395-4405.
45. Am S, Em A. Medicinal Plants with Antiviral Properties to Tackle Covid-19 Pandemic: A Short-Review. SunText Review of BioTechnology. 2021;02(01)..
46. Tripathi S, Murtuja S, Siddique MU, Ansari A, Rakshit G. Inhibitory Potency of Chlorogenic Acid from Apple Cider Vinegar Against Alzheimer's Disease: Molecular Docking and Dynamics Validation. Journal of the American Nutrition Association. 2024;44(3):267-282.
47. Alghamdi S, Alhaidal H, Mohammed A, Alsubait A, Alshammari M, Alsaqer L, et al. A Novel Integrated Approach: Plant-Mediated Synthesis, in vitro and in silico Evaluation of Silver Nanoparticles for Breast Cancer and Bacterial Therapies. International Journal of Nanomedicine. 2025;Volume 20:10043-10071.